Glucocorticoids and myosin5b loss of function induce heightened PKA signaling in addition to membrane traffic defects

Radia Forteza[a,†], M. Kaimul Ahsan[b,†], Fernando Cartón-García[c], Diego Arango[c], Nadia A. Ameen[b,*], and Pedro J. Salas[a,*]

[a]Department of Cell Biology, Miller School of Medicine, University of Miami, Miami, FL 33136; [b]Department of Pediatrics, Yale School of Medicine, Yale University, New Haven, CT 06510; [c]Group of Biomedical Research in Digestive Tract Tumors, CIBBIM-Nanomedicine, Vall d'Hebron University Hospital Research Institute (VHIR), Universitat Autónoma de Barcelona, 08035 Barcelona, Spain

ABSTRACT **Loss-of-function mutations in the nonconventional myosin Vb (Myo5b) result in microvillus inclusion disease (MVID) and massive secretory diarrhea that often begins at birth. Myo5b mutations disrupt the apical recycling endosome (ARE) and membrane traffic, resulting in reduced surface expression of apical membrane proteins. ARE disruption also results in constitutive phosphoinositide-dependent kinase 1 gain of function. In MVID, decreased surface expression of apical anion channels involved in Cl^- extrusion, such as cystic fibrosis transmembrane conductance regulator (CFTR), should reduce fluid secretion into the intestinal lumen. But the opposite phenotype is observed. To explain this contradiction and the onset of diarrhea, we hypothesized that signaling effects downstream from Myo5b loss of function synergize with higher levels of glucocorticoids to activate PKA and CFTR. Data from intestinal cell lines, human MVID, and Myo5b KO mouse intestine revealed changes in the subcellular redistribution of PKA activity to the apical pole, increased CFTR phosphorylation, and establishment of apical cAMP gradients in Myo5b-defective cells exposed to physiological levels of glucocorticoids. These cells also displayed net secretory fluid fluxes and transepithelial currents mainly from PKA-dependent Cl^- secretion. We conclude that Myo5b defects result in PKA stimulation that activates residual channels on the surface when intestinal epithelia are exposed to glucocorticoids at birth.**

Monitoring Editor
Keith E. Mostov
University of California, San Francisco

Received: Jul 2, 2018
Revised: Oct 22, 2019
Accepted: Oct 23, 2019

INTRODUCTION

Microvillus inclusion disease (MVID) is a severe congenital diarrhea that disproportionately affects infants of Navajo Indians in the United States (Oliva *et al.*, 1994; Sherman *et al.*, 2004). MVID patients will die rapidly due to uncontrolled secretory diarrhea (SD) unless they receive total parenteral nutrition support for life. Intestinal fluid loss from diarrhea often exceeds 140 ml/kg per d, resembling SD of cholera (Cutz *et al.*, 1989). At the ultrastructural level the disease is characterized by microvillus atrophy, subapical PAS-positive vesicles, and large vacuoles containing fully formed microvilli (microvillus inclusions [MI]) that appear in a fraction of mature enterocytes (Ameen and Salas, 2000). More than 40 loss-of-function mutations in myosin Vb (Myo5b) have been reported to cause MVID (van der Velde *et al.*, 2013). In addition, homozygous truncating mutations in syntaxin 3 (STX3) were also shown to result in a milder late-onset form of the disease (Wiegerinck *et al.*, 2014). The fact that impaired membrane traffic from apical recycling endosomes (AREs) to the surface is at the core of MVID pathophysiology was further demonstrated in constitutive (Cartón-García *et al.*, 2015) and conditional (Schneeberger *et al.*, 2015) homozygous Myo5b knockout mice, as well as in Rab8- (Sato *et al.*, 2007) and

This article was published online ahead of print in MBoC in Press (http://www.molbiolcell.org/cgi/doi/10.1091/mbc.E18-07-0415) on October 30, 2019.

†These authors contributed equally to this work.

*Address correspondence to: Pedro J. Salas (psalas@miami.edu); Nadia A. Ameen (nadia.ameen@yale.edu).

Abbreviations used: AC, adenylate cyclase; ARE, apical recycling endosome; CFTR, cystic fibrosis transmembrane conductance regulator; CFTR172, inhibitor of CFTR anion permeability; Cl^-, channel; FRET, fluorescence (or Förster) resonance energy transfer; GC, glucocorticoid; kd, knockdown; KO, knockout; MVID, microvillus inclusion disease (OMIM 251850); Myo5b, myosin Vb (unconventional); NHE3, sodium–hydrogen antiporter 3; ROI, region of interest.

Rab11- (Sobajima *et al.*, 2014) deficient mice, all of which mimic human MVID morphological features.

The Rab11/Slp4/Myo5b/Munc18 complex carries apically bound vesicles to the surface and mediates their binding to STX3, as a first step for membrane fusion. This pathway mediates apical delivery of a subset of apical membrane proteins including NHE3, the sodium–hydrogen exchanger that is necessary for sodium absorption in the small intestine, CFTR, and other apical membrane proteins (Vogel *et al.*, 2015). Apical surface expression of these proteins is severely decreased in MVID patients (Ameen and Salas, 2000; Kravtsov *et al.*, 2016). Yet, defects in this exocytic pathway lead to selectivity in apical protein targeting to the membrane. While there is a consensus that NHE3 is not expressed on the apical surface, alkaline phosphatase and sucrase isomaltase appear both on the surface and in subapical compartments (Ameen *et al.*, 2000). Furthermore, CFTR, the main Cl^- channel responsible for cAMP-dependent SD, is only partially decreased in human MVID intestine (Kravtsov *et al.*, 2016). It has been proposed that MVID diarrhea results from an imbalance of partially decreased CFTR (secretion) and totally absent NHE3 (absorption). However, an absence of NHE3 on the MVID enterocyte apical membrane cannot explain the magnitude of the SD in these patients, because NHE3-deficient mice (Schultheis *et al.*, 1998) and humans with congenital sodium diarrhea due to NHE3 mutations (Janecke *et al.*, 2015) display milder diarrhea even in the presence of normal CFTR expression. In fact, it is counterintuitive that decreased CFTR because of the Myo5b loss of function contributes to SD. In an effort to understand the nature of Na^+ and Cl^- stool losses in MVID diarrhea, the ion transport profile of human MVID small intestine was investigated by Rhoads and coworkers (Rhoads *et al.*, 1991). In brief, using Ussing chambers and jejunum tissues ex vivo, these investigators found a 3.2 mEq h^{-1} cm^{-2} decrease in net mucosal to serosal Na^+ flux, along with a 3.9 mEq h^{-1} cm^{-2} *increase* in net serosal-to-mucosal Cl^- flux. Basal jejunal Cl^- secretion in MVID tissues was found to be close to the maximal rate of normal tissues. While these results are totally consistent with a SD, they are still puzzling in the context of decreased CFTR. The decrease in Na^+ absorption can be explained by lack of NHE3 on the cell surface. However, the molecular mechanism for the Cl^- secretion remains unexplained.

In summary, there are two unanswered questions regarding the pathophysiology of MVID. First, it is paradoxical that *decreased* surface expression of CFTR results in massive SD. Second, there are two forms of MVID: early (shortly after birth) and late onset (during the first year). Unlike other congenital diarrheas such as down-regulated adenoma congenital Cl^- diarrhea (Choi *et al.*, 2009) or NHE3 (congenital secretory sodium diarrhea 8; Janecke *et al.*, 2015), early-onset MVID presents with low incidence of polyhydramnios (intrauterine diarrhea; Cutz *et al.*, 1989; Chen *et al.*, 2011). In other words, it is unclear why SD starts shortly after birth when the Myo5b mutations and the molecular machinery for intestinal secretory function are present well before birth.

The major mechanisms responsible for fluid secretion in SD include cAMP/PKA-dependent activation of CFTR in the proximal small intestine (mainly the jejunum) through two mechanisms: 1) direct phosphorylation of CFTR, which increases the open state of the channel; and 2) exocytic traffic of CFTR-associated subapical vesicles to increase the functional CFTR abundance on the brush border membrane (Ameen *et al.*, 1999; Ameen and Salas, 2000; Barrett and Keely, 2000; Golin-Bisello *et al.*, 2005). These CFTR phosphorylations occur in a tandem of at least eight phospho Ser/Thr in the regulatory domain, which are targets of PKA (Bozoky *et al.*, 2013). Importantly, once phosphorylated, the CFTR regulatory domain binds 14-3-3 proteins, which increase forward traffic to the cell surface (Liang *et al.*, 2012).

We have shown that the phosphoinositide-dependent kinase 1 (PDK1) is associated with the ARE in enterocytes (Mashukova *et al.*, 2012). As ARE vesicles enlarge and become disorganized and poorly polarized in MVID, a substantial fraction of PDK1 dissociates from the membrane and becomes loosely distributed in the cytoplasm (Kravtsov *et al.*, 2014). Cytosolic PDK1 can constitutively activate several kinases, including PKA (Kobayashi and Cohen, 1999; Nirula *et al.*, 2006; Pearce *et al.*, 2010; Tobias *et al.*, 2016). Thus, we speculated that increased CFTR secretory activity of a smaller number of channels due to cell-autonomous PKA activity could explain the MVID conundrum.

Glucocorticoids (GCs) exert diverse physiological actions and ensure salt and water homeostasis by multiple mechanisms: the classic slower genomic pathway involves GC binding to intracellular receptors to regulate gene transcription and translation resulting in protein synthesis. Thus, many GC effects are mediated by genomic up-regulation of serum glucocorticoid kinases in response to stress (Lang *et al.* 2018), which are activated by PDK1. Rapid nongenomic GC signaling of effector molecules involves activation of membrane-mediated secondary signaling cascades including cAMP and Ca^{++} (Mitre-Aguilar *et al.* 2015). Importantly, glucocorticoids dramatically increase within days preceding birth in mammalians (Fowden *et al.* 1998; Keller-Wood *et al.* 2009) resulting in profound transcriptional and signaling changes. For this reason, we focused on GC effects on Myo5b-deficient enterocytes as a possible explanation for the perinatal onset of the MVID phenotype.

Accordingly, our goal was to test the hypothesis that there are changes in intracellular signaling arising from Myo5b defects, which result in increased apical fluid secretion mediated by PKA and CFTR in the presence of the perinatal increase in GCs.

RESULTS

Two intestinal cell lines deficient in Myo5b display changes in PKA-dependent phosphorylation patterns that mimic MVID: effect of dexamethasone

CaCo2 cells (Muller *et al.*, 2008) and the subclone CaCo2BBe (C2BBe; Peterson and Mooseker, 1992), closely resemble villus enterocytes of the small intestine (Collaco *et al.*, 2010; Jakab *et al.*, 2011; Knowles *et al.*, 2014). Effective (>90%) silencing of Myo5b with lentivirus-delivered short hairpin (shRNA) constructs was regularly achieved (Figure 1A) after stringent selection in puromycin (Kravtsov *et al.*, 2016). Under these conditions, C2BBe cells display all the morphologic features of human MVID enterocytes including the loss of microvilli and the appearance of MI (Kravtsov *et al.*, 2014; Vogel *et al.*, 2015), which can be visualized as a steep decrease in apical phalloidin signal and intracellular phalloidin-positive inclusions in a fraction of the cells (Figure 1B, arrow).

To determine whether the activity of PKA is specifically exerted in the apical domain of epithelial cells, where CFTR molecules are localized, we used a widely validated antibody recognizing phosphorylated PKA consensus target sites. This antibody has been used in immunohistochemistry, immunofluorescence, and immunoblot assays in more than 40 publications. We validated this antibody by immunoblot of forskolin (cAMP)-stimulated C2BBe cell extracts and with a PKA inhibitor (Figure 1C and Supplemental Figure 1A). This antibody will be referred to as PKA p-substrate antibody hereafter. As expected, the antibody recognized several bands. Some bands appeared only in the forskolin-treated cells, while other bands increased in intensity under forskolin stimulation (Figure 1C). Because localization of PKA activity is highly regulated, we wanted

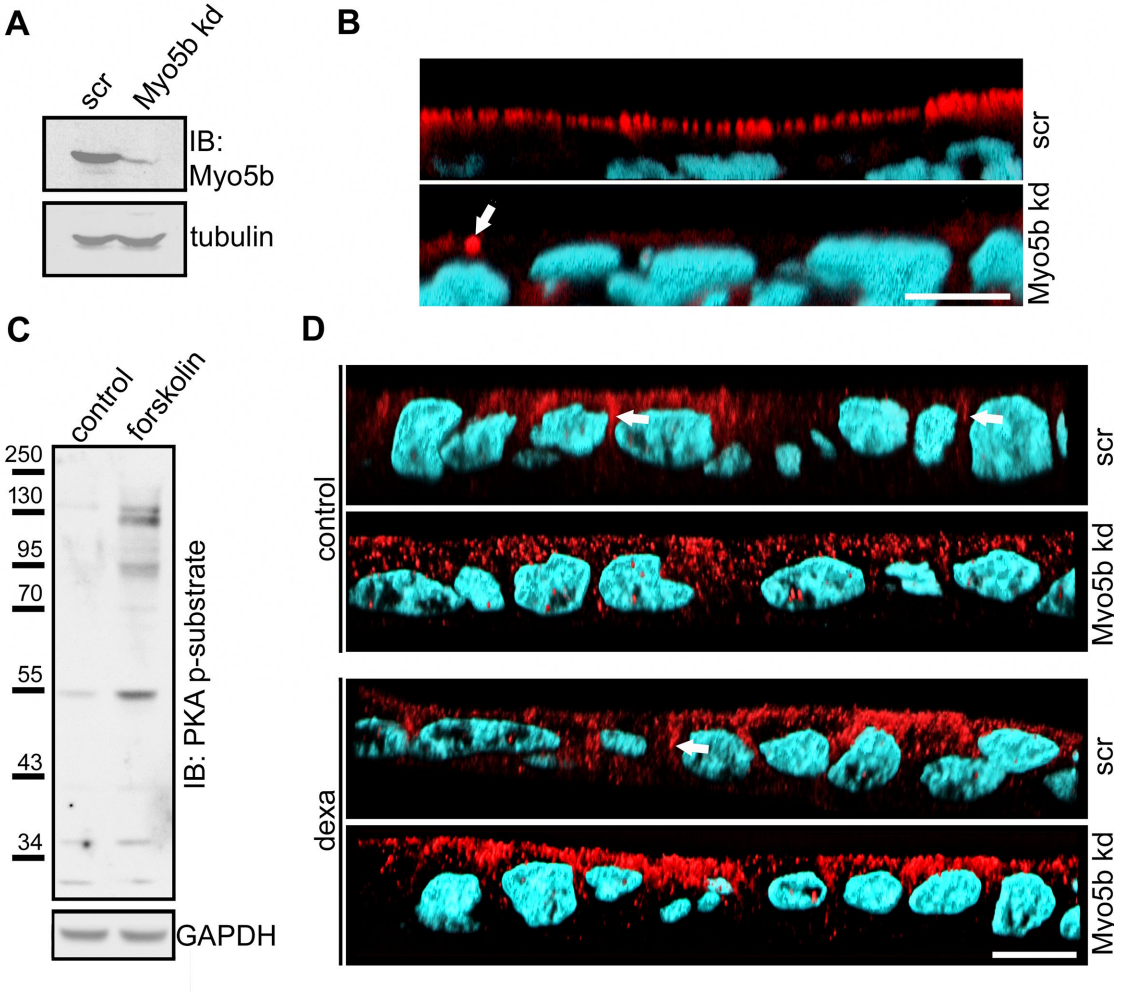

FIGURE 1: Myosin 5b knockdown and corticoids induce changes in the distribution of PKA activity in C2BBe intestinal epithelial cells. (A) C2BBe cells were transduced with lentivirus expressing a scrambled shRNA (scr, control) or anti-myosin 5b shRNA (Myo5b kd), extracted, and analyzed by immunoblot. (B) C2BBe cells (scr or Myo5b kd) were stained with fluorescent phalloidin (XZ plane from confocal stacks). Arrow, phalloidin-positive inclusion. Scale bar = 10 μm. (C) C2BBe cells were treated with 10 μM forskolin or vehicle (control) for 3 h. Immunoblots were processed with PKA p-substrate antibody (RRXpS/pT) or anti-GAPDH antibody. (D) Parallel cultures were processed for immunofluorescence with the same PKA p-substrate antibody (red channel, XZ plane). Scale bar = 10 μm.

to understand the distribution of PKA-phosphorylated targets in intestinal cells. C2BBe cells transduced with a scrambled RNA-expressing lentivirus (scr) showed mostly lateral membrane localization of PKA-phosphorylated proteins (Figure 1D, arrows) with many cells lacking apical signal. Myo5b knockdown (kd) or dexamethasone treatment of scr cells changed this distribution to a broadly cytoplasmic signal but did not result in a clear apical localization. However, in Myo5b kd cells previously treated with dexamethasone the signal was concentrated and enhanced at the apical domain (Figure 1D, bottom panel). Semiquantitative measurements of pixel intensities showed significantly increased signal in the apical domain and decreased signal in the basolateral region and cytoplasm (Supplemental Figure 1B).

Another epithelial intestinal cell line, T84, resembles intestinal crypt cells, and has been shown to closely mimic the electrophysiologic properties of secretory intestinal epithelia (Tousson *et al.*, 1996; Silvis *et al.*, 2009). These cells form tight junctions (Supplemental Figure 2A), albeit their differentiation is slower than C2BBe. They can also be grown in spheroids, which, after 2 wk in Matrigel, show mostly single-layered cysts, with only sporadic double-layered cells (Supplemental Figure 2B, arrows). Importantly, the cells appear polarized, but the lumens are usually collapsed, as expected from cells with a net absorptive fluid transport (Supplemental Figure 2B). We previously used electrophysiologic approaches to demonstrate stimulated CFTR ion transport activity in Myo5b-deficient T84 cells (Kravtsov *et al.*, 2016). Accordingly, these cells were used extensively in functional studies here (next section). In addition, we used T84 cells in the current studies as a second cell line to decrease the chance that the observations may be due to random changes in the genetic background or signaling related to transformation. The same lentivirus-delivered anti-Myo5b shRNA was used in T84 cells, resulting in a similar steep down-regulation of Myo5b (Figure 2C). Pixel intensities were quantified in regions of interest (ROIs) randomly localized at the apical domain by grid overlapping (example shown in the leftmost panel of Figure 2A, and the confocal level and depth of ROIs in Figure 2B). Unlike C2BBe cells, only apical PKA p-substrate signal was observed in T84 cells (Figure 2B). PKA-phosphorylated target showed minimal changes when scr cells were

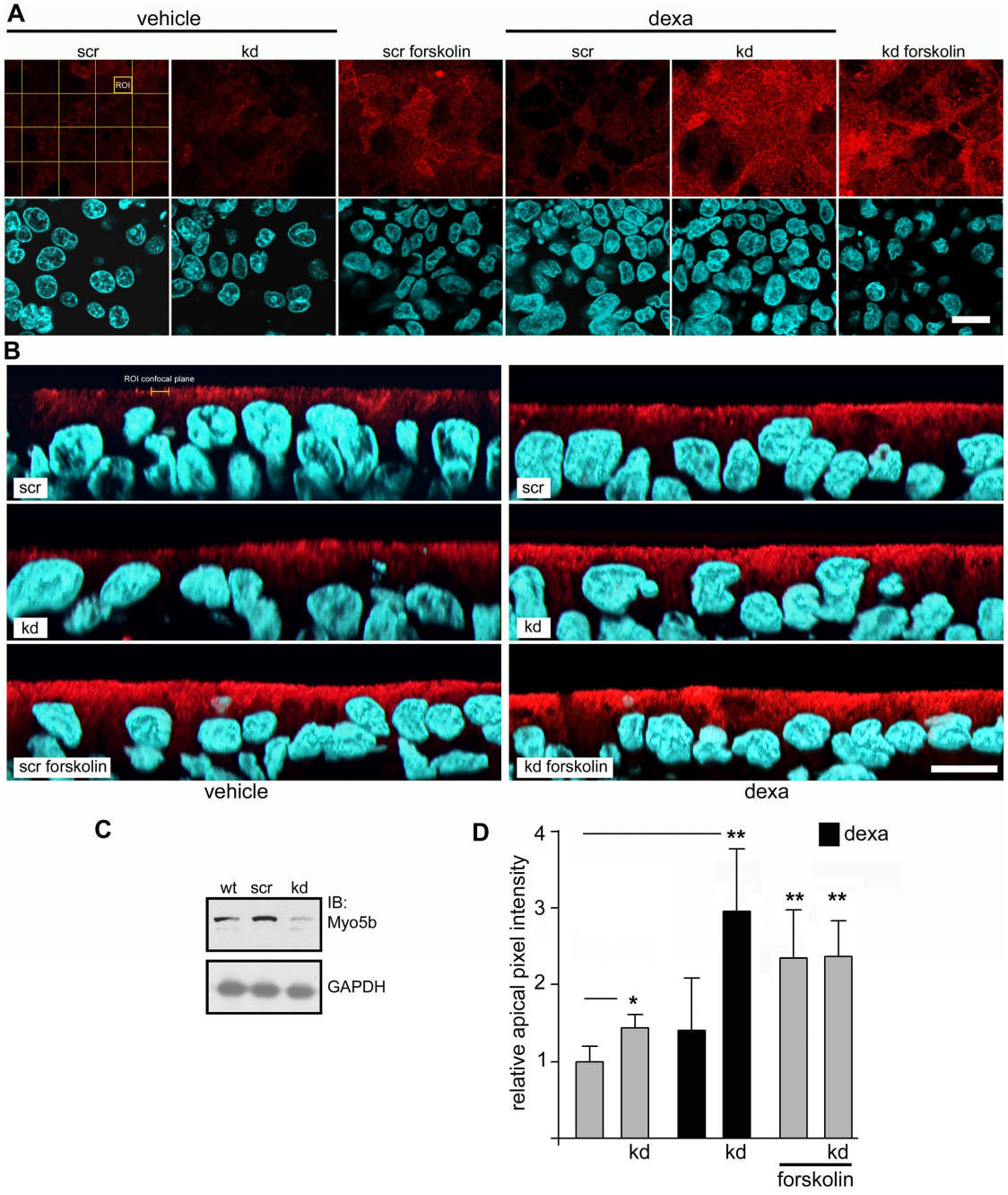

FIGURE 2: Myosin 5b knockdown and dexamethasone increase apical PKA-phosphorylated targets in T84 intestinal cells. (A) Immunofluorescence localization of proteins phosphorylated by PKA in scr or Myo5b kd (only kd is labeled in the graph) T84 cells were incubated vehicle (control) or with 0.5 μM dexamethasone for 10 d. As a positive control, parallel cultures, expressing scr or kd shRNA were also incubated in 10 μM forskolin for 3 h. Confocal XY images typical of three experiments at the apical focal plane (see B) shown for PKA p-substrate antibody signal (red), and the corresponding images in the transnuclear plane below for DAPI signal. Yellow rectangle: Example of ROI used for quantification in D. Unbiased random distribution of ROIs was ensured by overlapping a grid and placing ROIs at every other intersection. Scale bar = 10 μm. (B) XZ sections from the same experiment. Yellow line shows the focal plane of ROIs shown in A and the approximate focal depth (vertical lines). Scale bar = 10 μm. (C) T84 cells without transduction or selection (wt) or transduced with lentiviral particles expressing scrambled (scr, control) or anti-Myo5b (kd) shRNAs and selected, were analyzed for Myo5b expression by immunoblot to determine knockdown efficacy. (D) Random ROIs were placed on the apical domain in confocal (XY) sections of monolayers as shown in A by overlapping grid intersections. Several ROIs per image were taken. The average pixel intensities were calculated and normalized to the average in scr control cells. $n = 3$; *, $p < 0.05$; **, $p < 0.01$.

compared with Myo5b kd cells in the absence of dexamethasone (Figure 2, A and D). However, PKA substrate signal increased 2.5-fold when the cells were incubated with forskolin, regardless of Myo5b expression indicating that PKA is available and in active conformation in kd or scr controls. Importantly, average pixel intensities significantly increased threefold in Myo5b-deficient cells incubated

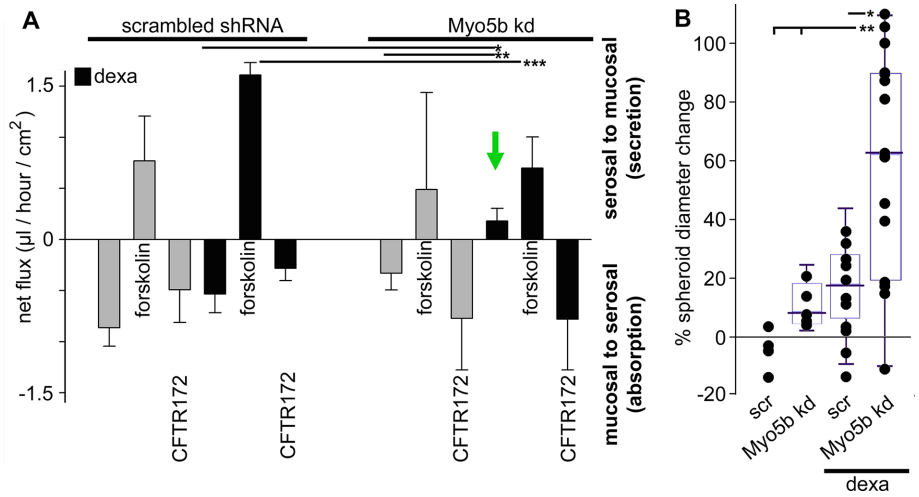

FIGURE 3: Myo5b kd and dexamethasone induce a fluid secretory phenotype in live unstimulated intestinal epithelial cells. (A) Transepithelial net fluid secretion in Myo5b kd T84 cells treated with dexamethasone. Gravimetric determinations of net fluid transport in T84 cells (grown on filters) show secretion in Myo5b KD cells when incubated in 0.5 µM dexamethasone (green arrow). This effect was blocked by 10 µM CFTR172. Control vs. pharmacologic treatments estimated by ANOVA; *, $p < 0.01$; **, $p < 0.02$; ***, $p < 0.05$; $n = 4$. NS, not significant. (B) T84 cells expressing scrambled shRNA (scr) or anti-Myo5b shRNA were grown in Matrigel for 10 d. The volume of the spheroids was measured as maximum caliper diameter at 4 and 27 h after adding 0.5 µM dexamethasone (dexa) or vehicle to the medium. Each dot represents the change in one spheroid. Relative changes in diameter are expressed as the percentage of increase (or decrease, –). *, $p < 0.001$; **, $p < 0.01$ (Kruskal-Wallis). Box-and-whisker plots are shown for categories with $n > 5$.

in the presence of dexamethasone, a level indistinguishable from the forskolin-positive control (Figure 2, A and D).

Myo5b-deficient intestinal epithelial cells show apical fluid and Cl^- secretion in the presence of dexamethasone that can be reversed by CFTR inhibitors

Fluid transport was measured in cells grown on filters by a gravimetric method as described before for C2BBe cells (Kravtsov *et al.*, 2014). These experiments were performed in T84 cells, because these cells express CFTR and display electrophysiologic features similar to those in the intestinal epithelium with Cl^- secretion more robust than other epithelial models including CaCo2 cells (Dharmsathaphorn *et al.*, 1984; Resta-Lenert and Barrett, 2002). The gravimetric method showed fluxes of similar magnitude to those obtained by others with different approaches (Toriano *et al.*, 2001). The spontaneous absorptive fluid flux average in T84 cells was 1 µl/h/cm^2 (mucosal to serosal; Figure 3A). As a comparison, the absorptive fluxes reported in C2BBe were 3.1 µl/h per cm^2 (Kravtsov *et al.*, 2014). This is consistent with crypt-like T84 cells as compared with villus-resembling absorptive C2BBe cells. As in the case of C2BBe, Myo5b kd decreased the absorptive flux, but did not revert it into a net secretory (serosal-to-mucosal) fluid flux. As a positive control for secretory response, forskolin induced a significant net fluid secretion in both control and Myo5b kd cells. The forskolin-induced response was decreased in Myo5b kd cells but not abolished (Figure 3A). This is expected for cells expressing only a fraction of the normal CFTR on the apical surface. These findings are consistent with previous electrophysiologic measurements of forskolin-stimulated CFTR anion currents in T84 cells deficient in Myo5b (Kravtsov *et al.*, 2016). They are also consistent with decreased swelling of forskolin-stimulated intestinal organoids generated from mice deficient in Myo5b grown in low GC levels (Schneeberger *et al.*, 2015). However, when the cells were grown in dexamethasone, the unstimulated Myo5b kd monolayers showed spontaneous fluid secretion at 27% of the maximum secretory flux in forskolin stimulation in KD cells, or 11% of the flux in forskolin-stimulated scr cells (Figure 3A, green arrow). Importantly, this serosal-to-mucosal net fluid flux was abolished by the specific CFTR inhibitor CFTR172 and was independent of secretagogues. Moreover, our finding of a net secretory flux of 0.8 µl/h per cm^2 in the Myo5b kd and dexamethasone condition may seem very small. However, considering that the secretory surface of the newborn small intestine is ~25,000 cm^2 (Struijs *et al.*, 2009), it is consistent with 480 ml fluid secretion per day. That is well within the volume range of diarrhea of a 3 kg MVID patient (Cutz *et al.*, 1989).

To independently corroborate fluid secretion, we used spheroid cultures of T84 cells in Matrigel. The diameter of the cysts grown for 10 d did not significantly change in a 23-h period, either in scr- or Myo5b kd cells (Figure 3B). Likewise, when scr T84 cells were supplemented with dexamethasone, the diameter change was <20% (Figure 3B and Supplemental Video_control). However, in Myo5b kd cultures supplemented with dexamethasone, the cysts significantly grew 62% (Figure 3B and Supplemental Video_dexa). These results support the hypothesis that Myo5b-defective cells secrete fluid in the presence of postnatal physiological levels of GCs.

To determine whether fluid secretion is due to CFTR-dependent apical Cl^- extrusion in epithelial cells deficient in Myo5b, standard electrophysiology experiments in an Ussing chamber were performed. Transepithelial electric current (Isc) is the result of a subset of cellular ion transport mechanisms which are electrogenic. CFTR-mediated Cl^- secretion is among them (Kato and Romero, 2011). First, T84 cells in tissue culture medium DMEM, were challenged with forskolin from the apical side. In scrambled shRNA-expressing cells, stimulation caused a robust increase in Isc, with a transient peak in the range 40–100 µA/cm^2, which decreased to a steady-state plateau after 15–20 min (Figure 4A). The Isc values at steady state less than the average of the currents in the absence of stimulation are quantified in Figure 4C. In all cases, Myo5b kd cells showed significantly less electrogenic response to forskolin. The forskolin response represents the maximum electrogenic activity induced by cAMP. Therefore, it reports on the total available apical anion channels responsive to PKA stimulation. Accordingly, this result indicated a reduction in the number of channels expected from the apical traffic defects resulting from the loss of Myo5b. However, it is important to notice that under Myo5b kd, forskolin-induced currents were reduced only to approximately half of the value in controls (Figure 4C), indicating that a substantial number of apical anion channels remain available for transport in Myo5b-defective cells.

Because multiple ion transport mechanisms coexist in intestinal epithelial cells, we wanted to simplify the number of electrogenic mechanisms by using a modified Ringer medium, without amino acids and supplemented with glucose on the basolateral side only, to supply energy. To eliminate the apical electrogenic Na^+/glucose

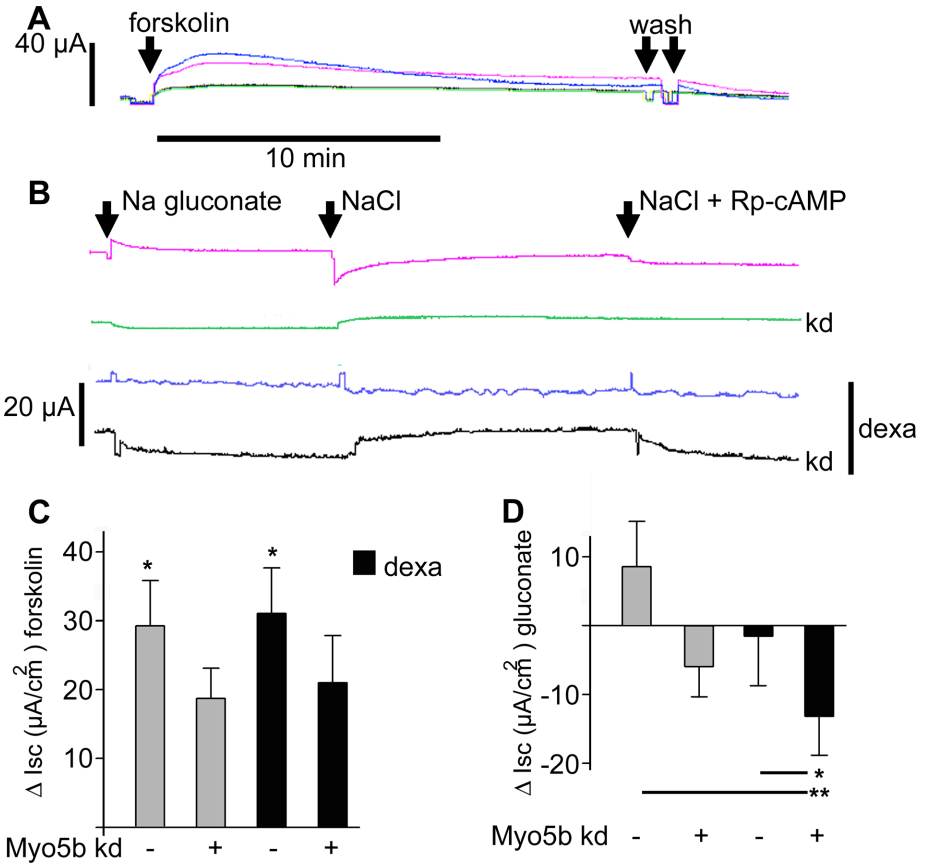

FIGURE 4: Myo5b kd and dexamethasone induce a Cl^- secretory phenotype in unstimulated intestinal cells. (A) Typical recordings of short circuit current (Isc) in confluent, differentiated T84 cells transduced with scrambled shRNA (blue and purple), or Myo5b antisense shRNA (green and black traces), grown on Snapwell filters and analyzed in an Ussing chamber in standard DMEM culture medium. Forskolin (0.5 μM) was added from the apical side only. Some cells had been incubated in the presence of 0.5 μM dexamethasone for 10 d (blue and black traces). (B) Typical recordings of Isc in confluent, differentiated T84 cells transduced with scrambled shRNA, or Myo5b antisense shRNA (colors as in A), grown on Snapwell filters and measured in an Ussing chamber in normal Cl^- Ringer solution (129.1 mM Cl^-), or low Cl^- Ringer solution (128 mM sodium gluconate, 1.1 mM Cl^-). For both Ringer formulations, the apical solution was supplemented with 10 mM mannitol while the basolateral solution contained 10 mM glucose. At the end of each experiment, the cells were incubated in normal Cl^- solution in the presence of 40 μM Rp-cAMP. (C) Quantification of experiments like the one shown in B. Measurements were taken around 15 min after adding forskolin, in steady state. The bars represent the difference between Isc (in μA/cm^2) in stimulated cells minus the baseline in the same experiment. Statistical significance was determined by *t* test; *, $p < 0.05$; $n = 4$. (D) Quantification of the experiments like the one in C. Bars represent the average difference between nonstimulated Isc (μA/cm^2) in normal Cl^- Ringer and low Cl^- (gluconate) Ringer. *, $p < 0.04$; **, $p < 0.02$; $n = 3$.

cotransport, glucose was replaced by mannitol on the apical side. Under these conditions, we asked how much of the basal, unstimulated current is carried by Cl^-. To that end, scrambled or Myo5b shRNA-expressing cells grown with or without dexamethasone, were sequentially measured in normal Cl^- Ringer, low Cl^- Ringer (gluconate), and back again in normal Ringer. In other words, Cl^- concentration was reduced on both sides of the membrane by 100-fold. The basal currents in normal Cl^- in all cases were small (3 ± 3.2 μA/cm^2). There were no statistically significant differences among all the conditions. Chloride replacement resulted in small changes in basal unstimulated currents, indicating that the current was not carried by Cl^-. The exceptions were Myo5b kd cells incubated in dexamethasone (Figure 4, B, black trace, and D). In this case, a statistically significant change in transepithelial current was observed, opposite to the current generated by electrogenic apical Cl^- secretion (e.g., Figure 4A, forskolin). Similar changes were observed when cells in normal Cl^- were supplemented with the PKA inhibitor Rp-cAMP, which blocks the cAMP binding site and is, therefore, highly specific for PKA (Figure 4B). These results support the notion that unstimulated Myo5b-defective intestinal cells display apical anion secretion driving isotonic fluid secretion under PKA signaling in the presence of dexamethasone.

PKA-dependent phosphorylated targets localize to the apical region in Myo5b KO mice and human MVID enterocytes

To confirm whether enhanced PKA activity in the apical domain of intestinal epithelial cells deficient in Myo5b is also observed in vivo, in nontransformed cells, we analyzed a Myo5b KO mouse model and human tissues from MVID patients.

The global Myo5b KO mouse model was previously described (Cartón-García *et al.*, 2015). The pups can suck milk but develop massive diarrhea with hypoglycemia and die within 12 h after birth. Accordingly, samples from these mice were obtained at the late fetal stage when intestinal crypts are not yet developed, and only immature villi are observed. Tissue sections were processed for immunohistochemistry (IHC) using the PKA p-substrate antibody described in Figure 1, C and D. In wild-type (wt) mice, signal appeared in enterocytes near the tip of villi. It was distributed to the cytoplasm and the lateral membrane, and, to some extent, to the apical membrane (Figure 5A, arrow). Conversely, the signal was mostly apical (Figure 5B, arrow) in Myo5b KO samples.

In non-MVID human biopsies, PKA p-substrate signal was diffuse, with a faint apical and lateral membrane concentration (Figure 5D, arrow). On the contrary, in MVID biopsies, the signal was restricted to the apical membrane (Figure 5E, arrow) and to intracellular apical structures consistent with the images of MIs (Figure 5E, arrowhead). In summary, Myo5b KO in a mouse model of MVID, and MVID in human intestine both result in changes in the subcellular distribution PKA-phosphorylated targets. The redistribution of PKA activity in murine and human Myo5b loss of function strongly resembles the observations in Myo5b kd C2BBe (Figure 1D and Supplemental Figure 1B) and T84 cells (Figure 2B). Of note, we conclude that the Myo5b defect results in apical PKA activity with decreased activity in the cytoplasm and lateral membrane and increased activity in the apical domain.

Apical cAMP concentration gradients appear in Myo5b-deficient cells incubated in dexamethasone

If the Myo5b loss-of-function effect on PKA activity has any functional implication in apical CFTR channel function, it must be

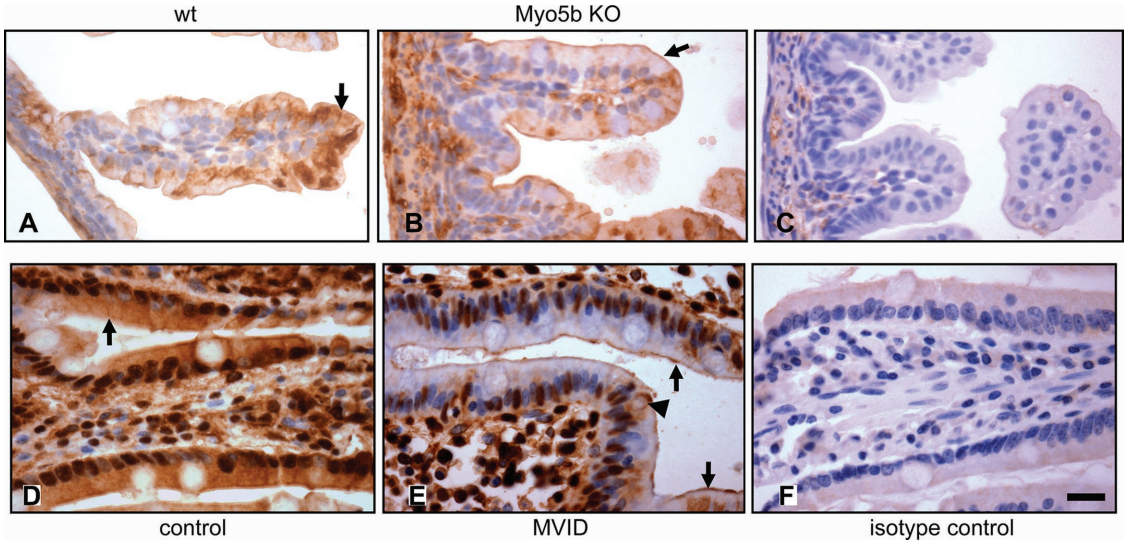

FIGURE 5: PKA-phosphorylated substrates concentrate under the apical domain in intestinal epithelia defective in Myo5b in vivo. (A–C) Fetal mouse small intestine, stained with PKA p-substrate antibody (A, B) or isotype control, processed with a similar dilution of nonimmune rabbit serum (C). (B) Sample from Myo5b KO mouse. (A, C) Heterozygous control. (D, E) Human duodenum biopsies from unrelated disease (D, F) or MVID (E). Both patients (6 and 5 mo old, respectively) were subjected to endoscopy and duodenal biopsy as diagnostic procedures for chronic diarrhea. Diagnosis of MVID was reached by PAS and EM (unpublished data), confirming the presence of MI (arrowhead). Arrows point at apical PKA p-substrate signal. Scale bar = 20 μm.

localized very close to the membrane. Confocal microscopy does not provide adequate resolution in the *z*-axis to make this assertion. Thus, the images in Figures 1 and 2 could represent PKA targets in subapical compartments, which are enlarged in Myo5b-deficient intestinal cells. Therefore, we wanted to examine whether PKA activity and cAMP localize in the vicinity of the apical CFTR channel (Ameen *et al.*, 2003) in Myo5b loss of function. We confirmed this in the human T84 cells expressing scrambled (scr) and anti-Myo5b shRNA. The latter showed increased colocalization of CFTR and PKA p-substrate signals (Figure 6A, merge). To verify whether this colocalization was within distances enabling molecular interaction, we performed fluorescence resonance energy transfer (FRET) determinations using fluorochromes CY3 and CY5 covalently linked to secondary antibodies. FRET efficiency was measured after acceptor (CY5) photobleaching in random ROIs in the apicalmost confocal optical section (Figure 6B). FRET efficiency was significantly increased 10-fold in Myo5b-deficient cells, preincubated in dexamethasone, as compared with cells expressing scrambled RNA (Figure 6C). While these experiments do not allow calculation of the Förster radius of interaction, we conclude that PKA-phosphorylated sites are concentrated within four immunoglobulin G (IgG) molecule lengths (~240 nm) of apical CFTR molecules as a result of the Myo5b defect and incubation in dexamethasone.

It is generally accepted that spatially restricted adenylate cyclase activity may result in submicron-sized cAMP microdomains, although the mechanisms to restrict cAMP diffusion remain subject to debate (Calebiro and Maiellaro, 2014).To independently test the hypothesis that PKA activity is increased in the apical domain of Myo5b-deficient cells, we transduced confluent T84 cultures with a cAMP upward fluorescence biosensor with high efficiency using a modified baculovirus that infects mammalian cells. Confluent fully polarized live cells were imaged 48 h after transduction. Low levels of fluorescence, mostly localized to the basolateral region and cytoplasm, were observed in cells expressing scrambled shRNA. However, the fluorescence increased dramatically 30 min following treatment with 10 μM forskolin in the same cells (Figure 7, A and B, scr; examples of the focal plane of ROIs a, apical, b, basal, and cytoplasmic are shown in yellow boxes). Noticeably, cAMP signal was distributed throughout the cytoplasm and not particularly concentrated under the apical domain in forskolin-stimulated cells. The cAMP signal was increased in the apical domain of Myo5b-deficient cells, especially when preincubated in dexamethasone (Figure 7, A and B, kd). It is important to notice that cAMP gradients were inverted from a cytoplasmic/basal larger than apical in nonstimulated cells, to apical larger than basal when Myo5b deficiency was concurrent with dexamethasone supplementation (Figure 7B, arrows). Also, this increase in apical cAMP was observed in the absence of exogenous stimulation other than dexamethasone (serum-free medium and no forskolin). This is consistent with the increase in apical PKA p-substrate signal described in the same region of the cell in two intestinal Myo5b kd cell lines, Myo5b KO mice, and human MVID enterocytes as shown in previous sections.

Myo5b defect along with dexamethasone increase PKA-dependent phosphorylation in apical membrane proteins in intestinal epithelial cells

To confirm that apical membrane proteins, which would include CFTR, are phosphorylated in PKA targeted sites, cells were screened by vectorial cell surface biotinylation (Rodriguez-Boulan *et al.*, 1989). Not all proteins can be biotinylated. Derivatization depends on the presence of primary amines in the amino acid side chains exposed to the extracellular milieu. Therefore, surface biotinylation provides a sampling of apical surface proteins that can be derivatized with sulfo-NHS-biotin. As expected from deficient apical membrane traffic, the surface expression of a subset of apical proteins decreased in C2BBe Myo5b-deficient cells. Some bands were undetectable in Myo5b kd cells, while others were only very moderately decreased (Figure 8A, stars). This result is consistent with previous observations that loss of Myo5b leads to selective apical traffic

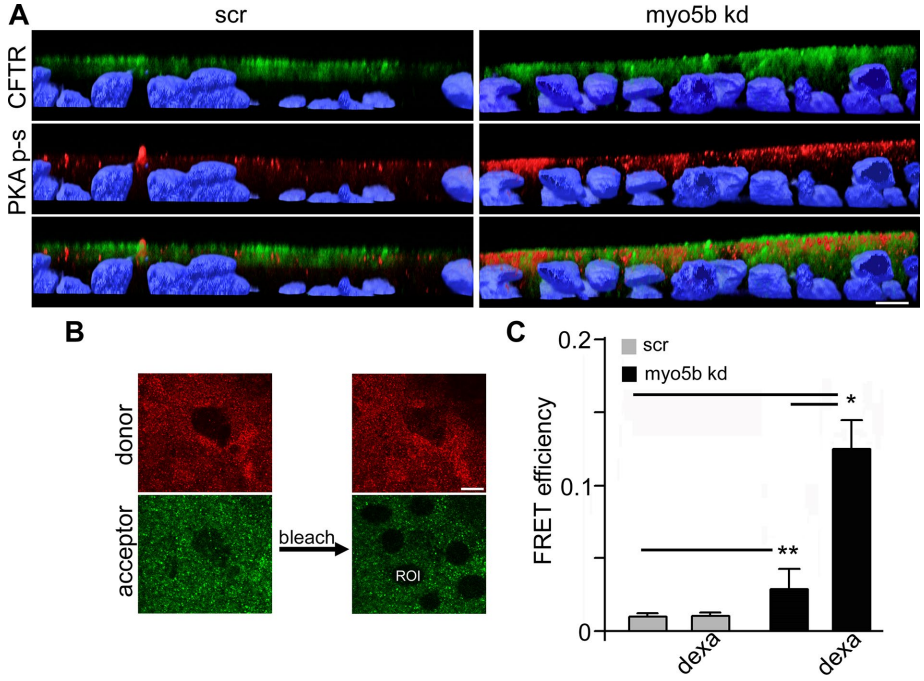

FIGURE 6: CFTR and PKA p-substrate signal colocalize within molecular distances in the apical domain in cells lacking Myo5b grown in the presence of 0.5 μM dexamethasone for 10 d (dexa). T84 cells were fixed and stained with anti-PKA p-substrate (p-s) antibody and anti-CFTR monoclonal antibodies, followed by affinity-purified antibodies labeled with Cy3 or Cy5. (A) Confocal stacks including the apical surface of the cells were imaged in the XZ plane. Scale bar = 10 μm. (B) In similar experiments, the apicalmost confocal section (0.68 μm thick in the *z*-axis) showing microvilli was subjected to acceptor (Cy5) bleaching (200 cycles) in random ROI and imaged again after bleaching. Scale bar = 4 μm. (C) Average FRET efficiency from three experiments (30 ROIs) is shown for control (scr) and Myo5b kd cells, incubated or not in dexamethasone (dexa) for 10 d. *, $p < 0.001$; **, $p < 0.04$.

defects differentially affecting individual apical membrane protein surface expression (Kravtsov *et al.*, 2016).

To extend this result to the other cell line and to understand the effect of Myo5b defect and GCs on apical membrane proteins, similar experiments were conducted. T84 cell cultures were incubated in dexamethasone (or vehicle) for 10 d. When Triton X-100 extracts of biotinylated (or not, control c) cells were analyzed, the decrease in apically exposed proteins in Myo5b kd was confirmed, but little or no effect of GCs was noticed (Figure 8B). To determine whether PKA targeting of biotinylated apical membrane proteins is affected by loss of Myo5b or corticoids, pull downs with streptavidin Sepharose beads followed by PKA p-substrate immunoblot were performed. Pull down resulted in enrichment in fewer bands phosphorylated by PKA, not readily noticeable in the total extract. No major bands were observed in the 140–200 kDa range, so we focused the analysis on two major bands with M_r 54 and 60×10^3 (Figure 8C, arrows) in the absence of GC supplementation; phosphorylation remained at similar levels in Myo5b-deficient cells. However, for cells grown in the presence of GC, Myo5b loss of function resulted in a statistically significant *increase* in phosphorylation (Figure 8, C and D). These results were quantified by densitometry of the two major bands (Figure 8D). Considering that expression of apical proteins *decreases* on the surface to various extents (Figure 8, B and C) because of membrane traffic defects dependent on Myo5b loss of function, these results indicate that proteins reaching the apical surface are exposed to a heightened PKA kinase activity in cells deficient in Myo5b and exposed to physiological levels of GCs.

The previous result raises the possibility that CFTR may be a target of PKA in the apical surface in Myo5b-deficient cells. To test that hypothesis, we took advantage of the previous work of various groups showing that 14-3-3 proteins associate with active CFTR through multiple PKA target phosphosites in tandem in the intrinsically disordered regulatory domain (Bozoky *et al.*, 2013) stabilizing the protein (Stevers *et al.*, 2016). Importantly, CFTR coimmunoprecipitates with 14-3-3, and co-ip is enhanced by forskolin (Liang *et al.*, 2012). In other words, 14-3-3β and CFTR coimmunoprecipitation is a reporter of PKA phosphorylation. In enterocytes and intestinal cell lines, 14-3-3β is expressed (Monroy, 2008; Gomez-Suarez *et al.*, 2016), along with isoforms ε, θ, ζ, and η. In addition, it has been shown that 14-3-3β heterodimerizes with ζ (Alvarez *et al.*, 2003) and ε (Ghorbani *et al.*, 2016). Because we did not determine the specific isoforms (homo- or heterodimers) involved in this coimmunoprecipitation, we will generically refer to 14-3-3 proteins hereafter. These proteins are abundant and cytosolic. The fraction bound to phosphorylated membrane proteins, thus, is expected to be relatively small. Accordingly, we enriched our extracts in membrane proteins by using Triton X-114 extraction, instead of the standard Triton X-100, followed by temperature separation of the detergent phase (Bordier, 1981; Taguchi and Schatzl, 2014). As predicted, Myo5b kd resulted in a steep increase in CFTR coimmunoprecipitation with 14-3-3 (Figure 8E). Interestingly, when this co-ip is driven by forskolin, both immature (b) and mature (glycosylated, c) forms of CFTR coimmunoprecipitate with 14-3-3 (Liang *et al.*, 2012). In the case of Myo5b kd cells, however, it was mostly the c form of CFTR that coimmunoprecipitated with 14-3-3, suggesting that phosphorylation occurred in a compartment beyond the Golgi apparatus. This result supports the notion that the fraction of CFTR that reaches the surface in Myo5b-defective epithelial cells is heavily phosphorylated in the regulatory domain in Myo5b-deficient cells, especially in the presence of GCs.

DISCUSSION

There is no question that MVID with Myo5b loss-of-function mutations is a disease resulting from defects in apically bound membrane traffic. This work shows that, in addition, the disorganization of the ARE compartment (Mashukova *et al.*, 2012; Kravtsov *et al.*, 2014) results in changes in intracellular signaling by PKA specifically in the microenvironment below the apical membrane. An apical gradient of cAMP, increased PKA-dependent phosphorylation in apical proteins, and CFTR–14-3-3 coimmunoprecipitation provide independent lines of evidence supporting this idea. Importantly, increased PKA activity was also confirmed in vivo in human MVID intestine and mouse Myo5b KO enterocytes, indicating that it is not a consequence of abnormal signaling pathways in transformed cell lines. Furthermore, because PKA activation is highly restricted to the apical membrane, and not global in the cell, it is likely due to effects on membrane-bound adenylate cyclases (ACs), phosphodiesterases,

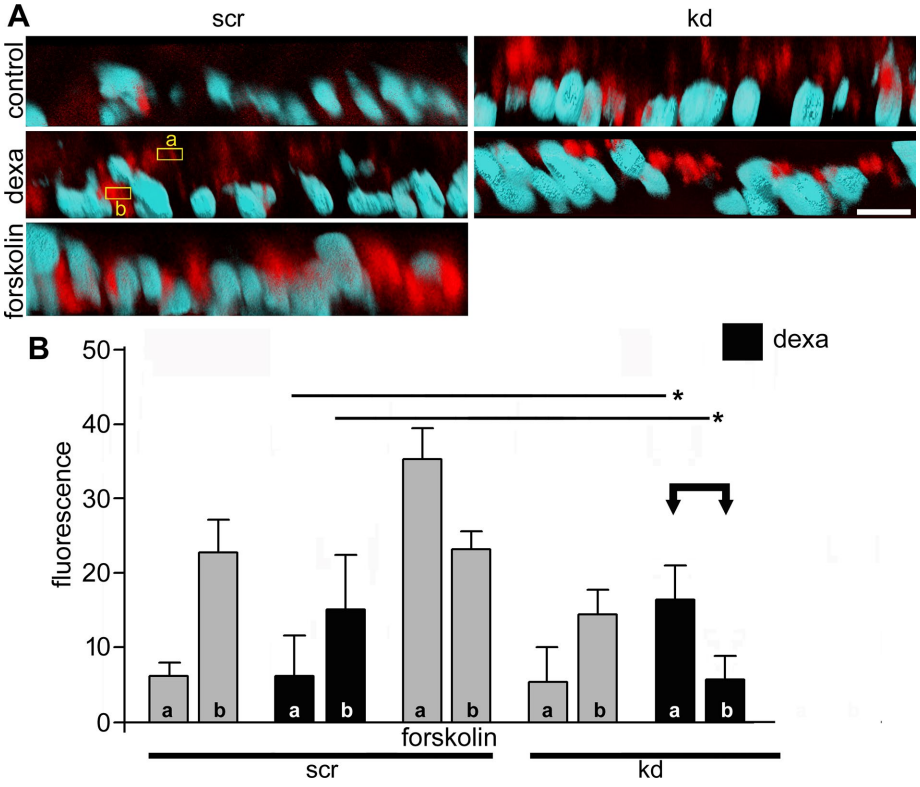

FIGURE 7: Myo5b loss of function induces redistribution of cAMP gradients in intestinal cells in the presence of GCs. Cyclic AMP was determined in vivo by transduction of a cAMP "upward" biosensor in T84 cells. Cells expressing a scrambled shRNA (scr) or Myo5b antisense shRNA (kd) were incubated in dexamethasone or vehicle as described before and transduced with a human-adapted baculovirus expressing cAMP biosensor. Some scr cell cultures (with no dexamethasone) were also preincubated with 10 μM forskolin for 30 min as a positive control for transduction and biosensor fluorescence. (A) 3D reconstruction of confocal stacks from live T84 cells show DNA counterstain (DAPI, blue) and biosensor fluorescence (red). Yellow rectangles are example focal planes of randomly localized apical (a) or basolateral (b) ROI in the XY sections used for quantification in B. Scale bar = 10 μm. (B) Biosensor fluorescence was quantified in positively transduced cells using random ROIs in the transnuclear/basolateral domain (b) and or in the apical domain (a) in XY confocal sections. Yellow rectangles show examples of the location of a and b confocal planes in XZ reconstructions. Arrows point at the only condition in which the apical/basolateral cAMP gradient is inverted in unstimulated (no forskolin) cells: Myo5b kd cells grown in dexamethasone. *, $p < 0.001$.

or specifically apical A-kinase anchoring proteins (Mies *et al.*, 2007). Substantial subapical localization of cAMP determined with a biosensor strongly supports the first two possibilities. It seems to be puzzling that Rhoads and coworkers (Rhoads *et al.*, 1991) found that octreotide, a known adenylate cyclase inhibitor, had no effect in two MVID patients treated for 1 d. This negative result, however, does contradict our conclusion. Octreotide inhibits ACs sensitive to Gαi G-proteins, which exclude group II ACs expressed in the intestine (Sabbatini *et al.*, 2014). Octreotide, for example, is not effective to control cholera diarrhea (Farthing, 2002), the paradigm of increased cAMP-dependent watery secretion. In summary, we conclude that the MVID diarrhea arises from the combined consequences of a complete loss of apical NHE3 (Ameen and Salas, 2000; Kravtsov *et al.*, 2016) and an incomplete decrease of apical CFTR, which is potentiated by PKA increased activity resulting in opening of resident CFTR channels still exposed on the surface.

Epithelial cells in culture commonly used in studies of the effect of Myo5b mutations (e.g., CaCo2 cells or enteroids) are not regularly supplemented with GCs. Cell lines would be grown in the presence of GCs from the serum, normally diluted to 5–10% of the physiological concentration. Enteroid defined media are not even supplemented with serum or GCs. Accordingly, the results found here have not been characterized in previous publications using cell lines or primary enteroid cultures. Specifically, poor responses to forskolin observed in the volume gain of enteroids derived from Myo5b floxed mice have been interpreted as negative evidence for increased CFTR function in MVID diarrhea. In those experiments, Schneeberger and coworkers found a ~1.5-fold increase in enteroid volume in normal cells as compared with Myo5b KO enteroids (Schneeberger *et al.*, 2015). Bearing in mind that the enteroids in that work were not specifically grown in dexamethasone, those experiments would have to be compared with our T84 cells, expressing scrambled or Myo5b shRNA in the presence of forskolin. In this study, we found that Myo5b kd results in a 47% decrease in the fluid secretion response to forskolin (Figure 3A) compared with the control cells. Likewise, Myo5b defects resulted in a similar decrease in apical electrogenic anion secretion (Figure 4, B and D). Our interpretation is that forskolin represents maximal cAMP stimulation, thus reflecting functionally the partial loss of CFTR on the surface. However, MVID patients would have no exogenous stimulation for cAMP levels. Instead, Myo5b loss of function compounded with GCs at levels that mimic the postpartum situation result in a cell-autonomous endogenously driven cAMP apical gradient and PKA stimulation that opens CFTR channels and results in Cl^- extrusion. In summary, the need of GCs pathway has been overlooked as an experimental variable in Myo5b-defective phenotypes and might be key to explain the timing of early-onset MVID. GCs exert many transcriptional and nontranscriptional effects. Understanding which one impacts on PKA activation in the Myo5b-defective background is beyond the scope of this work. However, currently there is no therapy for MVID diarrhea. This study suggests that the secretory component of MVID diarrhea could be reverted by modulating such PKA activation.

MATERIALS AND METHODS

Antibodies and reagents

Anti-PKA–phosphorylated substrate sites (PKA p-substrate, anti-RRXpS/pT) antibody was obtained from Cell Signaling (cat. # 9621S). The sources of other antibodies were as follows: GAPDH (Calbiochem; CB1001); tubulin (Abcam; ab52866); Myo5b (Novus Biologicals; NBP1-87746); ZO-1 MAb (ZO-1-1A12; ThermoFisher Scientific). CFTR monoclonal antibodies 596 and 769, against the NBD2 (C-terminal) domain (Kreda *et al.*, 2005; Cui *et al.*, 2007) were obtained from the Cystic Fibrosis Foundation, CFTR Antibody Distribution Program, University of North Carolina at Chapel Hill. Anti-14-3-3 (Proteintech; AB_2218096) was originally developed against full-length 14-3-3θ, but it cross-reacts with other 14-3-3

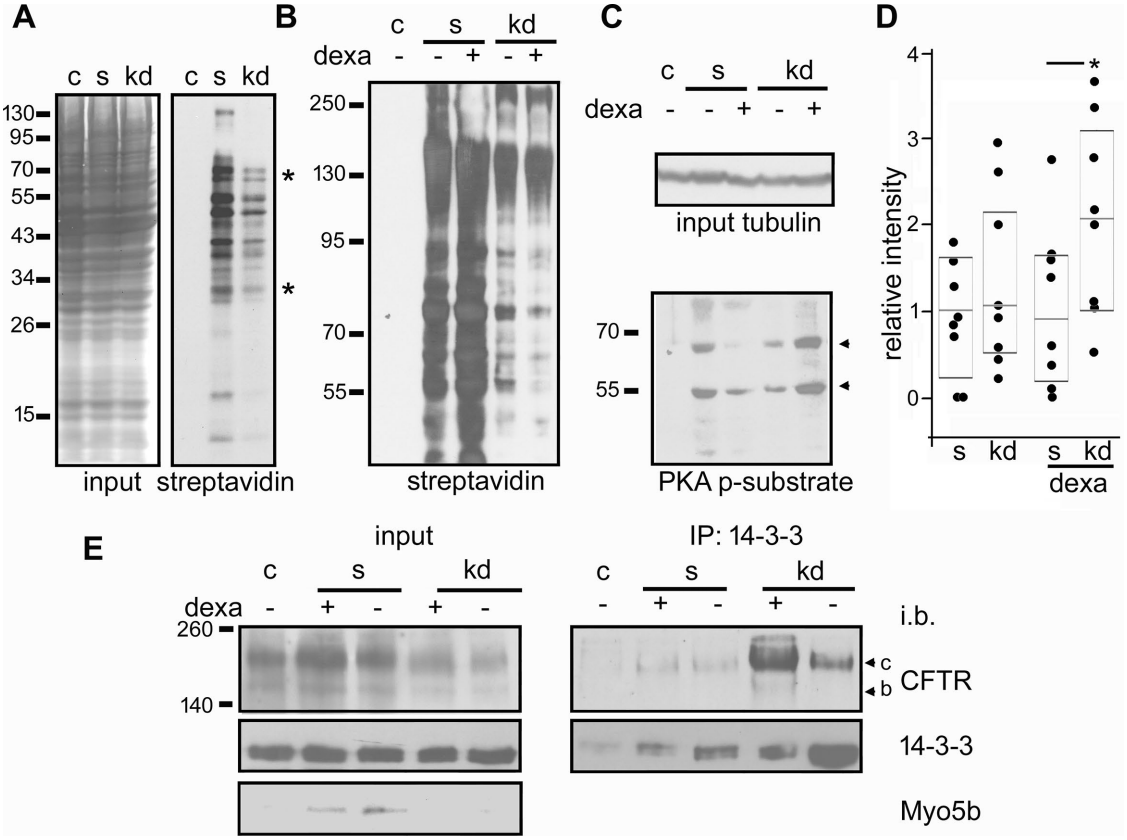

FIGURE 8: Biotinylated apical membrane protein epithelial cells deficient in Myo5b show increased phosphorylation. (A) C2BBe cells constitutively expressing scrambled shRNA (c and s) or Myo5b antisense shRNA (kd) were grown on filters, biotinylated from the apical side, extracted, pulled down with streptavidin-agarose, and visualized by blot and chemiluminescence with streptavidin. One set of cultures was not biotinylated (control, c). A fraction (10%) of the input was stained with Ponceau S red to show total protein (input). Stars indicate examples of biotinylated bands that remain exposed to the apical chamber in Myo5b-deficient cells (representative experiment out of three). (B) In similar experiments, T84 cells expressing scrambled RNA (s) or Myo5b shRNA (kd) were grown with or without 0.5 μM dexamethasone (dexa), and revealed with streptavidin-HRP. (C) A similar extract was pulled down with streptavidin beads and analyzed by immunoblot with PKA p-substrate antibody. A fraction (5%) of total cell extracts in Triton X-100 (input) was analyzed by immunoblot with anti-tubulin antibody as loading control. (D) Quantification of PKA p-substrate signal in two biotinylated bands. The PKA p-substrate signal relative to the average intensity of the bands in Myo5b-deficient cells with no dexamethasone treatment were plotted for the prominent 54 and 60 kDa bands shown in C. Box plots represent first, third quartile, and median for each group (each dot represents an independent observation). Kruskal-Wallis; *, $p < 0.02$. (E) T84 cells were treated as described in B. The cells were extracted in 2% Triton X-114 in the cold, and the extracts subjected to detergent condensation to enrich in membrane proteins and their binding partners. 10% of the input was analyzed by immunoblot (i.b.) with the antibodies listed on the right-hand side. The rest was immunoprecipitated with an anti–14-3-3 antibody recognizing multiple isoforms and analyzed for immunoblot with the same antibodies. For 14-3-3 blots, the signal was revealed with an anti-rabbit secondary antibody coupled to HRP that only recognizes the native conformation of IgG. Arrowheads in CFTR immunoblots point at the position of the immature (b) and mature (c) forms. M_r of standards are expressed $\times 10^{-3}$.

isoforms (Bai *et al.*, 2014) and has been validated for immunoprecipitation. Fluorescent secondary affinity-purified antibodies with minimal cross-reactivity were obtained from Jackson Immunoresearch Laboratories. ECL horseradish peroxidase (HRP)–conjugated affinity-purified antibodies were obtained from Amersham. TrueBlot HRP–anti-rabbit IgG antibody recognizing native conformation nonreduced protein was purchased from Rockland (TruBlot; 18-8816-31).

Cells and lentivirus

CaCo2 BBe(C2BBe) and T84 cells were obtained from the American Type Culture Collection. Lentivirus particles expressing anti-Myo5b shRNA or GFP were described before (Kravtsov *et al.*, 2014). Upon transduction, both cell types were continuously selected in 20 μg/ml puromycin. For experiments, the cells were kept in 12.5 μg/ml puromycin. Cells were kept for up to 10 passages after transduction or until the efficiency of knockdown was less than 90%. For experiments, C2BBe or T84 cells were grown on 3-μm-pore Transwell or Snapwell filters (Costar) for 2 wk after confluency, when C2BBe cells reach full differentiation. In preliminary experiments, we confirmed by reverse transcription-quantitative PCR that T84 cells also acquire the highest CFTR expression at that time.

T84 three-dimensional cultures (spheroids) in Matrigel (BD Biosciences) were prepared following the technique described elsewhere for Madin–Darby canine kidney cells (Martin-Belmonte *et al.*, 2008), and adapted for T84 cells (Bentz *et al.*, 2013). The spheroids

were used for experiments after 10 d in culture, with changes in media every other day.

Dexamethasone and pharmacological treatments

Synthetic glucocorticoid dexamethasone (Sigma) was kept in dimethyl sulfoxide (DMSO) stock solution for up to 3 mo at –20°C. Dexamethasone concentration in treatments was established on the basis of average blood cortisol concentrations in neonates, which range from 40 µg/l (~0.1 µM; Jonetz-Mentzel and Wiedemann, 1993) to 250 µg/l (~0.5 µM; Stevens, 1970), depending on the assays. Typically, cells were incubated in dexamethasone for 10 d before the day of the experiment to mimic the timing of the increase in serum GCs before birth.

Forskolin, Rp-cyclic 3′,5′-hydrogen phosphorothioate adenosine (Rp-cAMPS), and CFTR172 were purchased from Sigma. All these reagents, except Rp-cAMP, were kept in DMSO stock solutions at –20°C. Rp-cAMP stock solution was made in sterile phosphate-buffered saline (PBS) and frozen. H89 was purchased from Tocris.

Human samples were considered exempt nonhuman research on the basis that they were deidentified paraffin blocks retrieved from a repository.

Mouse intestine

The generation of the *Myo5b* knockout mouse model used has been described before (Cartón-García *et al.*, 2015). Mice heterozygous for the *Myo5b*-null allele were crossed and pregnant females were killed by CO_2 asphyxiation at day 20 of gestation. The embryos were obtained, kept on ice-cold PBS, and killed by decapitation. Tail clips were taken for DNA extraction and genotyping and the whole embryos were Formalin-fixed and paraffin-embedded as described (Cartón-García *et al.*, 2015).

IHC and immunofluorescence for PKA p-substrate antibody

Immunohistochemistry for the PKA p-substrate antibody was performed using the antigen retrieval protocol described by the manufacturer (www.cellsignal.com/products/primary-antibodies/phospho-ser-thr-pka-substrate-antibody/9621). Published data include validation by negative controls using phosphatases before tissue staining (same website). Independent validation of the use of this antibody for immunohistochemistry was published by others (Saitoh *et al.*, 2009). For immunofluorescence, the antibody was used after fixation in 10% trichloroacetic acid as described for other antibodies against phosphorylated epitopes (Hayashi *et al.*, 1999; Wald *et al.*, 2011).

Vectorial apical cell surface biotinylation was performed as described before (Rodriguez-Boulan *et al.*, 1989; Sargiacomo *et al.*, 1989). Briefly, confluent cell monolayers grown on Transwell filters were washed in PBS from the apical side only, leaving normal culture medium in the basal chamber. The cells were incubated on ice with 1 mM sulfo-NHS-LC-biotin (ThermoFisher Scientific; A39256) for 15 min, and then extensively washed with ice-cold DMEM. The cells were extracted in RIPA buffer in the presence of anti-proteases and anti-phosphatases. After centrifugation, the supernatants were incubated in streptavin-agarose beads (Sigma Chemical; S1638) for pull down. It must be noted that RIPA buffer extraction, while efficient for most membrane proteins has shown poor yields specifically for CFTR.

Immunoprecipitation of CFTR 14-3-3 complexes was performed as described before (Kravtsov *et al.*, 2012) but replacing Triton X-100 with 2% Triton X-114 to enrich for transmembrane 14-3-3 interactors, as described elsewhere (Bordier, 1981). It must be highlighted that CFTR is poorly extracted in RIPA buffer. An ad hoc CFTR extraction buffer (25 mM HEPES, 10% glycerol, pH 7.4, supplemented with protease inhibitors, HG) was used for these experiments as described before (Collaco *et al.*, 2010). In this buffer Triton X-114 clouding point is around 30°C. The 6% Triton X-114 HG stock solution was subjected to at least five cycles of condensation discarding the aqueous phase and replaced by freshly prepared HG buffer each time (Taguchi and Schatzl, 2014). This precondensed stock was diluted 1:3 in freshly prepared HG buffer before cell extraction (EB). Cell monolayers were washed with PBS on ice and extracted in EB for 15 min. The extracts were spun at 12,000 × *g* in the cold for 15 min and the supernatant was warmed to 33°C to separate the Triton X-114 phase (1 h). The aqueous supernatant was discarded, and the lower detergent phase resuspended in the same volume of cold HG buffer. Samples of this extract were taken as input. Incubation with the anti-14-3-3 antibody was performed in EB overnight at 4°C. Sepharose–protein A beads were prewashed in the same buffer for 1 h, spun, and added to the cell extracts for 3 h. Upon centrifugation, the beads were further washed in 1% Triton X-100 in PBS four times (1 h), and finally in 0.5M Tris buffer, pH 6.8, for 10 min. The protein was eluted in SDS sample buffer supplemented with 0.1% 2-mercaptoethanol at 37°C for 10 min. After separating the beads, the procedure was repeated one more time and the eluates were pooled.

cAMP biosensor

A cAMP upward mNeon Green cADDis biosensor (Tewson *et al.*, 2016) expressed under a CMV promoter was obtained from Montana Molecular (U0200G) and delivered by transduction with BacMam, a baculovirus modified to infect mammalian cells (Kost *et al.*, 2007). Fully differentiated T84 cell cultures (2 wk after confluency) grown on Transwell filters were transiently transduced with high efficiency by this vector. The cells were incubated in the presence of 2 mM sodium butyrate for 48 h after transduction according to the manufacturer's specifications before imaging. Six hours before imaging, 0.5 µg/ml 4′,6-diamino-2-phenylindole was added to the medium to contrast nuclei. Some cultures were supplemented with 10 µM forskolin for 30 min as positive control. Live cells were imaged in an inverted confocal microscope using a glass-bottom Petri dish. During imaging the cells were kept at 37°C and incubated in serum-free phenol red–free DMEM buffered with 20 mM HEPES.

Confocal microscopy

Confocal microscopy images were obtained in a Leica SP5 using an oil immersion 63× objective. For live-cell microscopy a water immersion 63× objective was used. Unless stated otherwise, the sections were collected at Airy = 0.9 or Airy = 1.2 for live cells to decrease laser intensity. For Airy 0.9, the section thickness was typically 0.6 µm and section spacing was 0.5 µm. For three-dimensional reconstructions, the stacks were imported into Slidebook software and cropped into 10-pixel-wide images. These images were reconstructed and rotated to show the *z*-axis. For quantification, ROIs were identified at random by overlapping a grid on the image in original (XY) images without rotation. To ensure that the measurements were performed at the apical domain, all the ROIs used for quantification comprised images of microvilli.

Live-cell microscopy was performed within a warmed chamber at 5% CO_2 using a Leica DMI6000 inverted microscope and a 20× objective. Time-lapse acquisition was done with LAS X software with images acquired every 15 min.

Fluorescence resonance energy transfer

FRET indexes were measured for the pair CY3-CY5 using the acceptor bleaching technique (Berney and Danuser, 2003; Centonze *et al.*, 2003). The method followed an established protocol for FRET

Collaco A, Marathe J, Kohnke H, Kravstov D, Ameen N (2010). Syntaxin 3 is necessary for cAMP- and cGMP-regulated exocytosis of CFTR: implications for enterotoxigenic diarrhea. Am J Physiol Cell Physiol 299, C1450–C1460.
Cui L, Aleksandrov L, Chang XB, Hou YX, He L, Hegedus T, Gentzsch M, Aleksandrov A, Balch WE, Riordan JR (2007). Domain interdependence in the biosynthetic assembly of CFTR. J Mol Biol 365, 981–994.
Cutz E, Rhoads JM, Drumm B, Sherman PM, Durie PR, Forstner GG (1989). Microvillus inclusion disease: an inherited defect of brush-border assembly and differentiation. New Engl J Med 320, 646–651.
Dharmsathaphorn K, McRoberts JA, Mandel KG, Tisdale LD, Masui H (1984). A human colonic tumor cell line that maintains vectorial electrolyte transport. Am. J Physiol 246, G204–G208.
Farthing MJ (2002). Novel targets for the control of secretory diarrhoea. Gut 50 (suppl 3), Iii15–Iii18.
Fowden AL, Li J, Forhead AJ (1998). Glucocorticoids and the preparation for life after birth: are there long-term consequences of the life insurance? Proc Nutr Soc 57, 113–122.
Ghorbani S, Fossbakk A, Jorge-Finnigan A, Flydal MI, Haavik J, Kleppe R (2016). Regulation of tyrosine hydroxylase is preserved across different homo- and heterodimeric 14-3-3 proteins. Amino Acids 48, 1221–1229.
Golin-Bisello F, Bradbury NA, Ameen NA (2005). Heat stable enterotoxin (STa) and cGMP stimulate CFTR translocation to the surface of villus enterocytes in rat jejunum and is regulated by protein kinase G. Am J Physiol Cell Physiol 289, C708–C716.
Gomez-Suarez M, Gutierrez-Martinez IZ, Hernandez-Trejo JA, Hernandez-Ruiz M, Suarez-Perez D, Candelario A, Kamekura R, Medina-Contreras O, Schnoor M, Ortiz-Navarrete V, *et al*. (2016). 14-3-3 proteins regulate Akt Thr308 phosphorylation in intestinal epithelial cells. Cell Death Differ 23, 1060–1072.
Hayashi K, Yonemura S, Matsui T, Tsukita S (1999). Immunofluorescence detection of ezrin/radixin/moesin (ERM) proteins with their carboxyl-terminal threonine phosphorylated in cultured cells and tissues. J Cell Sci 112 (Pt 8), 1149–1158.
Jakab RL, Collaco AM, Ameen NA (2011). Physiological relevance of cell-specific distribution patterns of CFTR, NKCC1, NBCe1, and NHE3 along the crypt-villus axis in the intestine. Am J Physiol Gastrointest Liver Physiol 300, G82–G98.
Janecke AR, Heinz-Erian P, Yin J, Petersen BS, Franke A, Lechner S, Fuchs I, Melancon S, Uhlig HH, Travis S, *et al*. (2015). Reduced sodium/proton exchanger NHE3 activity causes congenital sodium diarrhea. Hum Mol Genet 24, 6614–6623.
Jonetz-Mentzel L, Wiedemann G (1993). Establishment of reference ranges for cortisol in neonates, infants, children and adolescents. Europ J Clin Chem Biochem 31, 525–529.
Kato A, Romero MF (2011). Regulation of electroneutral NaCl absorption by the small intestine. Ann Rev Physiol 73, 261–281.
Keller-Wood M, von Reitzenstein M, McCartney J (2009). Is the fetal lung a mineralocorticoid receptor target organ? Induction of cortisol-regulated genes in the ovine fetal lung, kidney and small intestine. Neonatology 95, 47–60.
Knowles BC, Roland JT, Krishnan M, Tyska MJ, Lapierre LA, Dickman PS, Goldenring JR, Shub MD (2014). Myosin Vb uncoupling from RAB8A and RAB11A elicits microvillus inclusion disease. J Clin Invest 124, 2947–2962.
Kobayashi T, Cohen P (1999). Activation of serum- and glucocorticoid-regulated protein kinase by agonists that activate phosphatidylinositide 3-kinase is mediated by 3-phosphoinositide-dependent protein kinase-1 (PDK1) and PDK2. Biochem J 339 (Pt 2), 319–328.
Kost TA, Condreay JP, Ames RS, Rees S, Romanos MA (2007). Implementation of BacMam virus gene delivery technology in a drug discovery setting. Drug Discov Today 12, 396–403.
Kravtsov DV, Ahsan MK, Kumari V, van Ijzendoorn SC, Reyes-Mugica M, Kumar A, Gujral T, Dudeja PK, Ameen NA (2016). Identification of intestinal ion transport defects in microvillus inclusion disease. Am J Physiol Gastrointest Liver Physiol 311, G142–G155.
Kravtsov DV, Caputo C, Collaco A, Hoekstra N, Egan ME, Mooseker MS, Ameen NA (2012). Myosin Ia is required for CFTR brush border membrane trafficking and ion transport in the mouse small intestine. Traffic (Copenhagen, Denmark) 13, 1072–1082.
Kravtsov D, Mashukova A, Forteza R, Rodriguez MM, Ameen NA, Salas PJ (2014). Myosin 5b loss of function leads to defects in polarized signaling: implication for microvillus inclusion disease pathogenesis and treatment. Am J Physiol Gastrointest Liver Physiol 307, G992–G1001.
Kreda SM, Mall M, Mengos A, Rochelle L, Yankaskas J, Riordan JR, Boucher RC (2005). Characterization of wild-type and ΔF508 cystic fibrosis transmembrane regulator in human respiratory epithelia. Mol Biol Cell 16, 2154–2167.
Lang F, Stournaras C, Zacharopoulou N, Voelkl J, Alesutan I. (2018). Serum- and glucocorticoid-inducible kinase 1 and the response to cell stress. Cell Stress 3, 1–8.
Liang X, Da Paula AC, Bozoky Z, Zhang H, Bertrand CA, Peters KW, Forman-Kay JD, Frizzell RA (2012). Phosphorylation-dependent 14-3-3 protein interactions regulate CFTR biogenesis. Mol Biol Cell 23, 996–1009.
Martin-Belmonte F, Yu W, Rodriguez-Fraticelli AE, Ewald AJ, Werb Z, Alonso MA, Mostov K (2008). Cell-polarity dynamics controls the mechanism of lumen formation in epithelial morphogenesis. Curr Biol 18, 507–513.
Mashukova A, Forteza R, Wald FA, Salas PJ (2012). PDK1 in apical signaling endosomes participates in the rescue of the polarity complex atypical PKC by intermediate filaments in intestinal epithelia. Mol Biol Cell 23, 1664–1674.
Mies F, Spriet C, Heliot L, Sariban-Sohraby S (2007). Epithelial Na^+ channel stimulation by n-3 fatty acids requires proximity to a membrane-bound A-kinase-anchoring protein complexed with protein kinase A and phosphodiesterase. J Biol Chem 282, 18339–18347.
Mitre-Aguilar IB, Cabrera-Quintero AJ, Zentella-Dehesa A (2015). Genomic and non-genomic effects of glucocorticoids: implications for breast cancer. Int J Clin Exp Pathol 8, 1–10.
Monroy FP (2008). Toxoplasma gondii: effect of infection on expression of 14-3-3 proteins in human epithelial cells. Exp Parasitol 118, 134–138.
Muller T, Hess MW, Schiefermeier N, Pfaller K, Ebner HL, Heinz-Erian P, Ponstingl H, Partsch J, Rollinghoff B, Kohler H, *et al*. (2008). MYO5B mutations cause microvillus inclusion disease and disrupt epithelial cell polarity. Nat Genet 40, 1163–1165.
Nirula A, Ho M, Phee H, Roose J, Weiss A (2006). Phosphoinositide-dependent kinase 1 targets protein kinase A in a pathway that regulates interleukin 4. J Exp Med 203, 1733–1744.
Oliva MM, Perman JA, Saavedra JM, Young-Ramsaran J, Schwarz KB (1994). Successful intestinal transplantation for microvillus inclusion disease. Gastroenterology 106, 771–774.
Pearce LR, Komander D, Alessi DR (2010). The nuts and bolts of AGC protein kinases. Nat Rev Mol Cell Biol 11, 9–22.
Peterson MD, Mooseker MS (1992). Characterization of the enterocyte-like brush border cytoskeleton of the C2BBe clones of the human intestinal cell line, Caco-2. J Cell Sci 102 (Pt 3), 581–600.
Resta-Lenert S, Barrett KE (2002). Enteroinvasive bacteria alter barrier and transport properties of human intestinal epithelium: role of iNOS and COX-2. Gastroenterology 122, 1070–1087.
Rhoads JM, Vogler RC, Lacey SR, Reddick RL, Keku EO, Azizkhan RG, Berschneider HM (1991). Microvillus inclusion disease. In vitro jejunal electrolyte transport. Gastroenterology 100, 811–817.
Rodriguez-Boulan E, Salas P, Sargiacomo M, Lisanti M, Lebivic A, Sambuy Y, Vega-Salas D, Graeve L (1989). Methods to estimate the polarized distribution of surface antigens in cultured epithelial cells. Methods Cell Biol 32, 37–56.
Sabbatini ME, Gorelick F, Glaser S (2014). Adenylyl cyclases in the digestive system. Cell Signal 26, 1173–1181.
Saitoh S, Terada N, Ohno N, Saitoh Y, Soleimani M, Ohno S (2009). Immunolocalization of phospho-Arg-directed protein kinase-substrate in hypoxic kidneys using in vivo cryotechnique. Med Mol Morphol 42, 24–31.
Sargiacomo M, Lisanti M, Graeve L, Le Bivic A, Rodriguez-Boulan E (1989). Integral and peripheral protein composition of the apical and basolateral membrane domains in MDCK cells. J Membr Biol 107, 277–286.
Sato T, Mushiake S, Kato Y, Sato K, Sato M, Takeda N, Ozono K, Miki K, Kubo Y, Tsuji A, *et al*. (2007). The Rab8 GTPase regulates apical protein localization in intestinal cells. Nature 448, 366–369.
Schneeberger K, Vogel GF, Teunissen H, van Ommen DD, Begthel H, El Bouazzaoui L, van Vugt AH, Beekman JM, Klumperman J, Muller T, *et al*. (2015). An inducible mouse model for microvillus inclusion disease reveals a role for myosin Vb in apical and basolateral trafficking. Proc Natl Acad Sci USA 112, 12408–12413.
Schultheis PJ, Clarke LL, Meneton P, Miller ML, Soleimani M, Gawenis LR, Riddle TM, Duffy JJ, Doetschman T, Wang T, *et al*. (1998). Renal and intestinal absorptive defects in mice lacking the NHE3 Na^+/H^+ exchanger. Nat Genet 19, 282–285.
Sherman PM, Mitchell DJ, Cutz E (2004). Neonatal enteropathies: defining the causes of protracted diarrhea of infancy. J Pediatr Gastroenterol Nutr 38, 16–26.
Silvis MR, Bertrand CA, Ameen N, Golin-Bisello F, Butterworth MB, Frizzell RA, Bradbury NA (2009). Rab11b regulates the apical recycling of

the cystic fibrosis transmembrane conductance regulator in polarized intestinal epithelial cells. Mol Biol Cell 20, 2337–2350.
Snapp EL, Hegde RS (2006). Rational design and evaluation of FRET experiments to measure protein proximities in cells. Curr Protoc Cell Biol Chapter 17, Unit 17.19.
Sobajima T, Yoshimura S, Iwano T, Kunii M, Watanabe M, Atik N, Mushiake S, Morii E, Koyama Y, Miyoshi E, Harada A (2014). Rab11a is required for apical protein localisation in the intestine. Biol Open 4, 86–94.
Stevens JF (1970). Plasma cortisol levels in the neonatal period. Arch Dis Child 45, 592–594.
Stevers LM, Lam CV, Leysen SF, Meijer FA, van Scheppingen DS, de Vries RM, Carlile GW, Milroy LG, Thomas DY, Brunsveld L, Ottmann C (2016). Characterization and small-molecule stabilization of the multisite tandem binding between 14-3-3 and the R domain of CFTR. Proc Natl Acad Sci USA 113, E1152–E1161.
Struijs MC, Diamond IR, de Silva N, Wales PW (2009). Establishing norms for intestinal length in children. J Ped Surg 44, 933–938.
Taguchi Y, Schatzl HM (2014). Small-scale Triton X-114 extraction of hydrophobic proteins. Bio-Protocol 4, doi: 10.21769/BioProtoc.1138.
Tewson PH, Martinka S, Shaner NC, Hughes TE, Quinn AM (2016). New DAG and cAMP sensorso for live-cell assays in automated laboratories. J Biomol Screen 21, 298–305.
Tobias IS, Kaulich M, Kim PK, Simon N, Jacinto E, Dowdy SF, King CC, Newton AC (2016). Protein kinase Cζ exhibits constitutive phosphorylation and phosphatidylinositol-3,4,5-triphosphate-independent regulation. Biochem J 473, 509–523.
Toriano R, Kierbel A, Ramirez MA, Malnic G, Parisi M (2001). Spontaneous water secretion in T84 cells: effects of STa enterotoxin, bumetanide, VIP, forskolin, and A-23187. Am J Physiol Gastrointest Liver Physiol 281, G816–G822.
Tousson A, Fuller CM, Benos DJ (1996). Apical recruitment of CFTR in T84 cells is dependent on cAMP and microtubules but not calcium or microfilaments. J Cell Sci 109, 1325–1334.
van der Velde KJ, Dhekne HS, Swertz MA, Sirigu S, Ropars V, Vinke PC, Rengaw T, van den Akker PC, Rings EH, Houdusse A, van Ijzendoorn SC (2013). An overview and online registry of microvillus inclusion disease patients and their MYO5B mutations. Hum Mutat 34, 1597–1605.
Vogel GF, Klee KM, Janecke AR, Muller T, Hess MW, Huber LA (2015). Cargo-selective apical exocytosis in epithelial cells is conducted by Myo5B, Slp4a, Vamp7, and Syntaxin 3. J Cell Biol 211, 587–604.
Wald FA, Forteza R, Diwadkar-Watkins R, Mashukova A, Duncan R, Abreu MT, Salas PJ (2011). Aberrant expression of the polarity complex atypical PKC and non-muscle myosin IIA in active and inactive inflammatory bowel disease. Virchows Arch 459, 331–338.
Wiegerinck CL, Janecke AR, Schneeberger K, Vogel GF, van Haaften-Visser DY, Escher JC, Adam R, Thoni CE, Pfaller K, Jordan AJ, *et al*. (2014). Loss of syntaxin 3 causes variant microvillus inclusion disease. Gastroenterology 147, 65–68.e10.